

Article

Migration of Leaked Oil Vapor in Underground Water-Sealed Oil Storage Cavern Considering the Influence of Fractures

Dong Tang^{1,2,*} , Huixiang Jian¹, Min Song³ and Zhongming Jiang^{1,4}

¹ School of Hydraulic and Environmental Engineering, Changsha University of Science & Technology, Changsha 410114, China

² Key Laboratory of Offshore Geotechnics and Material of Zhejiang Province, College of Civil Engineering and Architecture, Zhejiang University, Hangzhou 310058, China

³ HydroChina ZhongNan Engineering Corporation, Changsha 410014, China

⁴ Key Laboratory of Water-Sediment Sciences and Water Disaster Prevention of Hunan Province, Changsha 410114, China

* Correspondence: tangdong@csust.edu.cn

Abstract: During the operation of underground water-sealed oil storage caverns, a large amount of oil vapor is generated due to volatilization. Oil vapor can easily leak into the surrounding rock, and fractures in the surrounding rock are usually the dominant channels for oil vapor leakage. To study the influence of fractures on oil vapor leakage and migration in underground water-sealed oil storage caverns during the oil storage period, a gas–liquid two-phase flow model of the fracture–pore dual medium in fractured rock mass was established. The program was implemented on the COMSOL platform by using weak-form PDE (partial differential equation). Then, taking an underground water-sealed cavern of an oil reserve as an example, the influence of the characteristic parameters of a single fracture on the evolution process of oil vapor leakage and migration during the oil storage period of the underground water-sealed oil storage cavern was studied. The results were further applied to the Huangdao underground oil depot project. The results show that the spatial distribution of oil vapor leakage is mainly affected by fractures. Through parameter sensitivity analysis, it was found that the geometric characteristic parameters of fractures will have a certain impact on the migration field of oil vapor leakage in underground caverns. Specifically, fracture permeability (k_f), fracture width (d_f), and fracture inclination (θ) are positively correlated with oil vapor leakage parameters (oil vapor leakage range and leakage volume), while the distance between the fracture and the middle cavern (s) is negatively correlated with oil vapor leakage parameters (oil vapor leakage range and leakage volume). The relative influence of fracture geometry parameters on the migration process of oil vapor leakage during the oil storage period of the underground water-sealed oil storage cavern is in the following order: $k_f > d_f > s > \theta$. Engineering application shows that the existence of fractures affects the spatial distribution of oil vapor leakage and migration, and the relationship between oil vapor leakage parameters and oil storage operation time is a positive power function. The gas–liquid two-phase flow model of the fracture–pore dual medium in fractured rock mass developed in this study could offer a numerical simulation tool to assess and mitigate the risk of oil vapor leakage. The research conclusions can provide some references for related problems encountered in similar projects.

Keywords: underground water-sealed petroleum cavern; two-phase flow; fracture–pore dual medium; oil vapor leakage; weak form



Citation: Tang, D.; Jian, H.; Song, M.; Jiang, Z. Migration of Leaked Oil Vapor in Underground Water-Sealed Oil Storage Cavern Considering the Influence of Fractures. *J. Mar. Sci. Eng.* **2023**, *11*, 1248. <https://doi.org/10.3390/jmse11061248>

Academic Editor: Merv Fingas

Received: 13 May 2023

Revised: 11 June 2023

Accepted: 13 June 2023

Published: 19 June 2023



Copyright: © 2023 by the authors. Licensee MDPI, Basel, Switzerland. This article is an open access article distributed under the terms and conditions of the Creative Commons Attribution (CC BY) license (<https://creativecommons.org/licenses/by/4.0/>).

1. Introduction

Underground water-sealed oil storage caverns have gradually become the preferred choice for many countries to realize economic and safe oil storage [1,2]. Low-freezing-point crude oil stored in underground water-sealed oil storage caverns produce and volatilize a large amount of oil vapor during the filling and emptying process, which leads to an

increase in storage pressure in the caverns. When the storage pressure is greater than the water pressure around the cavern, the oil vapor accumulated at the top of the cavern leaks into the surrounding rock and even into the atmosphere, which may lead to potential health, safety, and environmental problems [3]. The surrounding rock of most underground water-sealed oil storage caverns is mainly crystalline rock mass, and the permeability coefficients of the fractures and rock blocks normally differ by several orders of magnitude. With lower permeability coefficients, rock blocks restrict fluid flow, making the fractures the main path for seepage through the surrounding rock [4]. Moreover, due to the difference in the spatial distribution and development density of the fractures, the fractured rock mass has significant heterogeneity and anisotropy [5]. Therefore, it is necessary to study the influence of fractures on the seepage field and the leaked oil vapor migration process.

Researchers have conducted many studies on gas leakage in the surrounding rock matrix of underground caverns. The gas leakage after roof salt rock collapse and roof gypsum collapse was simulated and analyzed by the numerical simulation method [6]. Based on the characteristics of low dip angle and layered rock salt interlayer structure, the gas leakage analysis model of the salt cavern was established, and the gas leakage and migration law of deep strata around layered salt cavern underground storage were revealed [7]. Considering the effective parameters such as the hydrogeological characteristics of rocks and the physical and chemical properties of hydrocarbons, all possible scenarios of the two-phase mixed model were numerically simulated based on the full factorial design. On this basis, the genetic programming method was used to establish the prediction equation of gas leakage in Iran's unlined crude oil caverns [3]. The migration characteristics of gas under different water curtain pressures and the influence of water curtain pressure on the water seal performance of the cavern were discussed, and the engineering risk was evaluated from the perspective of water sealing [8,9]. The above research does not consider the influence of fractures in rock mass on gas leakage, so the obtained results have limited reference significance for practical engineering.

In practical engineering, the surrounding rock of underground caverns is mainly crystalline rock mass. Due to the long-term and complex geological structure, there are always a large number of fractures. The fracture network of underground rock mass constructed by a large number of fractures is complex. A single crack is the basic component of a complex fracture network [5]. Therefore, the study of gas leakage in complex fracture networks can start from the study of gas leakage in single fracture rock mass. Researchers have also conducted many studies on fractured rock mass. A two-dimensional three-phase flow model of an underground liquefied petroleum gas (LPG) cavern in Japan was established. Considering the influence of a single fault zone, the leakage and migration process of gas in the cavern was simulated, and the influence of the unsaturated fault zone on gas leakage and migration was discussed [10]. It was assumed that there is an unsaturated fracture connecting the cavern and the surface in the surrounding rock of the underground cavern. The numerical simulation method was used to simulate the influence of unsaturated fracture on the gas leakage and migration during the oil storage period of the cavern [11]. Based on an actual salt cavern gas storage project, the influence of the fault dip angle and distance between the fault and adjacent caverns on the safety of adjacent caverns is discussed by numerical simulation [12]. A hydrogeological model of an underground water-sealed cavern was established, and the seepage field of the cavern under the condition of fracture passing through the cavern area was analyzed [13]. An efficient unconfined seepage analysis method for analyzing fluid flow in the fractured rock mass was proposed. The method was applied to the underground oil storage project of unlined rock caverns, and the water sealing effect of the water curtain system in the fractured rock mass was studied [14]. The effect of fractures on the evolution of CO₂ plume during injection in salt-bearing layers was studied [15]. The influence of the water curtain system on the water-sealing effect of the cavern in fractured rock mass during the construction stage and oil storage stage was systematically analyzed by using a three-dimensional discrete fracture pipe network model [16]. The numerical technique based on a migration tracking algorithm

and path analysis was used to calculate the occurrence of gas migration in fractures around the underground unlined cavern through a discrete fracture network [17]. Computational fluid dynamics (CFD) has found practical applications in simulating multi-phase flow in porous media, particularly within the oil and gas industry, due to significant advancements in computer power. Wijeratne and Halvorsen [18] presented a numerical study on heavy oil reservoir flow with water drive, where they investigated the fingering phenomenon using the volume of fluid (VOF) method. Farahani et al. [19] proposed a pore-scale model to simulate the migration of fine particles through synthetic 2D porous media. Movahedi et al. [20] developed a CFD model to simulate single and two-phase fluid flow in two- and three-dimensional perforated porous media, considering various perforation geometries. It can be seen that previous studies have focused on the influence of fractures on water sealing and gas leakage mechanisms but often neglected the influence of different fracture characteristic parameters on the overall migration and evolution of oil vapor leakage during the oil storage operation of underground caverns.

In this paper, based on a large-scale underground water-sealed oil storage construction project in China and the theory of gas–liquid two-phase flow in porous media, a fracture–pore dual media two-phase flow model was developed by using the weak form of PDE based on the COMSOL platform. The numerical simulation of oil vapor leakage and migration during the operation of underground water-sealed oil storage considering the fracturing effect was carried out, and the influence of different fracture parameters on the oil vapor leakage and migration characteristics of underground water-sealed oil storage was simulated and further applied to the actual project of Huangdao in China. The research results can provide a theoretical reference for the design of water-sealed oil storage cavern and the treatment of fractures.

2. Theory and Calculation Scheme

2.1. Gas–Liquid Two-Phase Flow Model of the Fracture–Pore Dual Medium in the Fractured Rock Mass

In underground water-sealed oil storage caverns, a large amount of oil vapor accumulates at the top of the cave due to crude oil evaporation and other effects, which increases the pressure of oil vapor on the top of the cavern, and the increase in oil vapor pressure will make the oil vapor drive the groundwater in surrounding rocks or fractures to flow. This process can be described by the theory of gas–liquid two-phase flow in a fracture–pore dual medium.

Assuming that the water flows in the rock blocks and fractures in the fractured rock mass satisfies Darcy’s law, and there is an exchange of water and oil vapor between the rock blocks and the fractures, the governing equation adopted in the coupled mathematical model of seepage oil vapor migration in the fractured rock mass is as follows:

The flow of two-phase fluids in rock blocks can be described using the governing equations of phase transfer in porous medium and Darcy’s law.

(1) The water balance equation in porous rock blocks is:

$$\rho S_m \frac{\partial p}{\partial t} + \nabla \cdot \rho \left(-\frac{k_m}{\mu} (\nabla p + \rho \mathbf{g}) \right) = 0 \tag{1}$$

where ρ is the fluid density (kg/m^3), S_m is the water storage coefficient of the rock block ($1/\text{Pa}$), p is the fluid pressure (Pa), k_m is the permeability of the rock mass (m^2), μ is the fluid dynamic viscosity ($\text{Pa}\cdot\text{s}$), and \mathbf{g} is the gravity acceleration vector (m/s^2).

(2) The phase transfer equation in porous rock blocks is:

$$\frac{\partial}{\partial t} (\varepsilon_p \rho_i s_i) + \nabla \cdot (\rho_i \mathbf{u}_i) = 0 \tag{2}$$

where ε_p is the porosity of the porous medium (dimensionless), and \mathbf{u}_i is the volumetric flux of phase i (m/s). The i can take values w and g , representing liquid phase and gas phase,

respectively, satisfying $s_w + s_g = 1$. The volumetric flux is determined by an extended Darcy’s law:

$$\mathbf{u}_i = -\frac{k_{ri}}{\mu_i} k_m (\nabla p_i - \rho_i \mathbf{g}) \tag{3}$$

where ρ_i is the fluid density (kg/m^3), μ_i is the hydrodynamic viscosity, ($\text{Pa}\cdot\text{s}$), k_{ri} the relative permeability (dimensionless), k_m is the permeability of porous medium (m^2), and p_i is the fluid pressure (Pa).

The governing equations of two-phase fluid in the fractured medium can be deduced from the governing equations in the porous medium.

(3) The water balance equation in the fractures is:

$$d_f \rho S_f \frac{\partial p}{\partial t} + d_f \nabla_T \cdot \rho \left(-\frac{k_f}{\mu} (\nabla_T p + \rho \mathbf{g}) \right) = 0 \tag{4}$$

where d_f is the fracture width (m), d_f is the fracture water storage coefficient ($1/\text{Pa}$), and k_f is the fracture permeability ($\text{Pa}\cdot\text{s}$). ∇_T represents the derivative along the tangent direction of the crack.

(4) The phase transfer equation of porous medium in the fractures is:

$$\frac{\partial}{\partial t} (d_f \varepsilon_f \rho_i s_i) + \nabla_T \cdot (d_f \rho_i \mathbf{u}_i) = 0 \tag{5}$$

$$\mathbf{u}_i = -\frac{k_{ri}}{\mu_i} k_f (\nabla_T p_i - \rho_i \mathbf{g}) \tag{6}$$

where ε_f is the fracture porosity.

(5) Auxiliary equation

The auxiliary equations for fractures and porous medium are the same: The capillary pressure is the pressure difference between different phases and is a function of the saturation of the wetted phase. Scholars at home and abroad have deduced the relationship between relative permeability and capillary pressure based on experimental data. It has been found that they are all functions of the saturation of the wetting phase. Brooks and Corey [21] obtained an empirical relationship describing the drainage process through the inlet capillary pressure and the saturation of the wetted phase:

$$p_c = p_{s_g} - p_{s_w} \tag{7}$$

$$p_c(s_w) = p_{ec} \bar{s}_w^{-1/\lambda_p} \tag{8}$$

where p_c is the capillary pressure (Pa), p_{s_g} and p_{s_w} are the gas phase pressure and liquid phase pressure (Pa), respectively, p_{ec} is the inlet capillary pressure (Pa), \bar{s}_w is the average water saturation in the porous medium (dimensionless), and λ_p is the pore size distribution index, representing the curvature of the saturation characteristic curve, dimensionless.

In the Brooks–Corey model, the relative permeability of the two phases is given by:

$$\bar{s}_w = (s_w - s_{rw}) / (1 - s_{rg} - s_{rw}) \tag{9}$$

$$\bar{s}_g = (s_g - s_{rg}) / (1 - s_{rg} - s_{rw}) \tag{10}$$

$$k_{rw} = \bar{s}_w^{(3+2/\lambda_p)} \tag{11}$$

$$k_{rg} = \bar{s}_g^2 \left(1 - (1 - \bar{s}_g)^{(1+2/\lambda_p)} \right) \tag{12}$$

where, k_{rw} and k_{rg} are the relative permeability of the water phase and gas phase respectively (dimensionless), s_w and s_g are the saturation of water phase and gas phase respectively (dimensionless), s_{rw} and s_{rg} are the residual saturation of water phase and gas phase, respectively (dimensionless), and \bar{s}_g is the average saturation of gas phase (dimensionless).

In COMSOL Multiphysics, Darcy’s law interface is only applicable to single-phase fluid flow in the porous medium. To simulate two-phase flow, the coupling interface of multiphase flow in the porous medium which combines the physical fields of Darcy’s law

and the phase transfer can be used. The density and dynamic viscosity of the two-phase fluid can be expressed by the following equations:

$$\bar{\rho} = \sum_i s_i \rho_i \tag{13}$$

$$\bar{\mu} = \frac{\bar{\rho}}{\sum_i \frac{k_{ri} \rho_i}{\mu_i}} \tag{14}$$

where $\bar{\rho}$ is the average density of the fluid (kg/m³), and $\bar{\mu}$ is the average viscosity of the fluid (Pa · s).

2.2. Numerical Realization and Verification of the Model

COMSOL Multiphysics 6.0 (COMSOL, Inc., Burlington, MA, USA) is a software that employs the finite element method to simulate and solve partial differential equations (PDEs), enabling the analysis of various real physical phenomena. The software accommodates any PDE by expressing it in a weak form, which typically corresponds to the integral equation representation of the original strong form equation (differential equation). In COMSOL, users can input the coefficients and parameters of the calculation equation through the settings of the physical field. This customization allows for the precise specification of variables required for the simulation. Following the setup of coefficients and parameters, the software proceeds with the calculation of the built-in variables associated with each physical field. Subsequently, the weak form is utilized to combine these variables, enabling the solution of the dependent variables associated with each partial differential equation. By utilizing this approach, COMSOL facilitates the simulation and analysis of a wide range of physical phenomena, providing insights into complex systems and aiding in the understanding and optimization of various engineering and scientific processes.

In this study, COMSOL Multiphysics was used to solve the above equations. Among them, the rock block part could be realized in Darcy’s law and the porous medium phase transfer module with solid elements, and the fractured part could be realized by specifying a weak form partial differential equation for the boundary element.

At present, the COMSOL porous medium and groundwater flow analysis module have their own porous medium two-phase seepage interface, but this seepage analysis module does not have the calculation function of the fracture–pore dual medium two-phase seepage analysis. To realize this process of two-phase seepage in the fracture–pore dual medium in COMSOL, the secondary development of the multiphase flow interface in the porous medium is required. In this study, the weak form was used for the secondary development of the two-phase seepage analysis method in the porous medium; thus, the two-phase seepage analysis in the fractured medium was realized in the COMSOL software.

According to the COMSOL weak form expression, the boundary weak form equations of the fracture two-phase flow equations can be expressed by the following equations.

$$0 = -d_f \rho S_f \frac{\partial p}{\partial t} test(p) + d_f \rho \cdot \frac{dtang u}{dtang x} test\left(\frac{dtang p}{dtang x}\right) + d_f \rho \cdot \frac{dtang u}{dtang y} test\left(\frac{dtang p}{dtang y}\right) \tag{15}$$

$$0 = -d_f \frac{\partial(\epsilon_f \rho_{s_i} s_i)}{\partial t} test(s_i) + d_f \rho_{s_i} \cdot \frac{dtang u_i}{dtang x} test\left(\frac{dtang s_i}{dtang x}\right) + d_f \rho_{s_i} \cdot \frac{dtang u_i}{dtang y} test\left(\frac{dtang s_i}{dtang y}\right) \tag{16}$$

$$0 = -d_f \frac{\partial \epsilon_f (\rho_{s_1} s_1 + \rho_{s_2} s_2 - \rho)}{\partial t} test(p) + d_f test\left(\frac{dtang p}{dtang x}\right) \cdot \left[\frac{\partial X}{\partial x} \cdot N_x + \frac{\partial X}{\partial y} \cdot N_y - \rho \frac{dtang u}{dtang x} \right] + d_f test\left(\frac{dtang p}{dtang y}\right) \cdot \left[\frac{\partial Y}{\partial x} \cdot N_x + \frac{\partial Y}{\partial y} \cdot N_y - \rho \frac{dtang u}{dtang y} \right] + d_f Q test(p) \tag{17}$$

where X, Y is the material coordinate system; x, y is the space coordinate system, a coordinate transformation from the space coordinate system to the material coordinate system is required; N is the total mass flux; $\text{kg}/(\text{m}^2 \cdot \text{s})$; $test$ is a trial function operator which is used in the weak form of the equation; $dtang$ is an operator to compute components of the gradient of an expression projected onto the plane tangent to the boundary where the evaluation takes place; $dtang(p, x)$ is the tangential differential of the variable p on the boundary on the spatial dimension x ; and $dang(p, y)$ is the variable p on the boundary in tangential differential on the spatial dimension y .

The development process consists of two steps. (1) Define the boundary calculation variables in COMSOL. The purpose of defining the boundary calculation variable is to calculate various state variables related to the two-phase flow in the fracture. The definition of the variable needs to be an identifiable variable in the porous medium so that the flow exchange between the porous medium and the fractured medium can be achieved. The variable calculation logic is the dismantling of the constitutive structure of the two-phase flow equation. (2) Define the computational relationship between boundary calculation variables through the weak form of the boundary.

The example in [15] was used to verify the correctness of the numerical model of two-phase flow in the fracture-pore dual medium. In this example, gas injection in the saturated fractured porous medium was studied. The geometry of the model is shown in Figure 1. The size of the model is $1 \times 1 \text{ m}$, and there is a vertical crack in the middle with an equivalent hydraulic aperture of 5 mm .

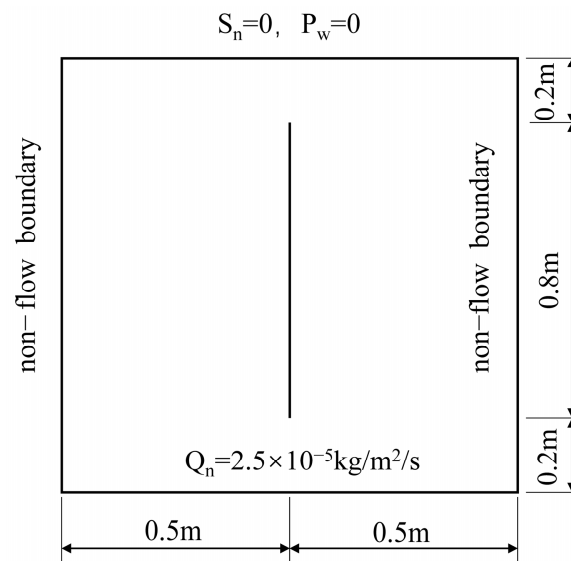


Figure 1. Geometry and boundary conditions of the two-phase flow model.

The parameters used in the simulation which are from [15] were as follows. The dynamic viscosity and density of water were $10^{-3} \text{ Pa}\cdot\text{s}$ and $1000 \text{ kg}/\text{m}^3$, respectively, while the dynamic viscosity of the gas phase was $1.65 \times 10^{-5} \text{ Pa}\cdot\text{s}$, and the density of the gas phase can be obtained by $P_n/84,149.6 \text{ kg}/\text{m}^3$, where P_n was the phase pressure of gas phase n . The intrinsic permeability of the fracture and porous matrix was 10^{-8} and 10^{-12} m^2 , respectively. The porosity of the two materials was also different, with a fracture porosity of 0.3 and a matrix porosity of 0.1.

Among the parameters used to calculate capillary pressure and relative permeability, only the capillary inlet pressure of the fracture and porous matrix differed. The capillary inlet pressure of the fracture was 1 kPa , while the capillary inlet pressure of the matrix was 2 kPa . The residual saturations of both the aqueous and gas phases in the fracture and matrix were zero, and the pore size distribution exponent λ was 2 for both materials.

The initial conditions of the whole area were $S_n = 0$ and $P_w = 0$, respectively. The boundary conditions at the top of the model were Dirichlet boundaries, which was $S_n = 0$,

$P_w = 0$; the boundary conditions at the bottom of the model were Neumann boundaries with a gas injection rate of $2.5 \times 10^{-5} \text{ kg/m}^2/\text{s}$; and the other two boundaries were no-flow Neumann boundaries.

Figure 2 is the distribution of water saturation at different times. It is consistent with the results of [15]. Thus, the rationality of the method in this study was confirmed.

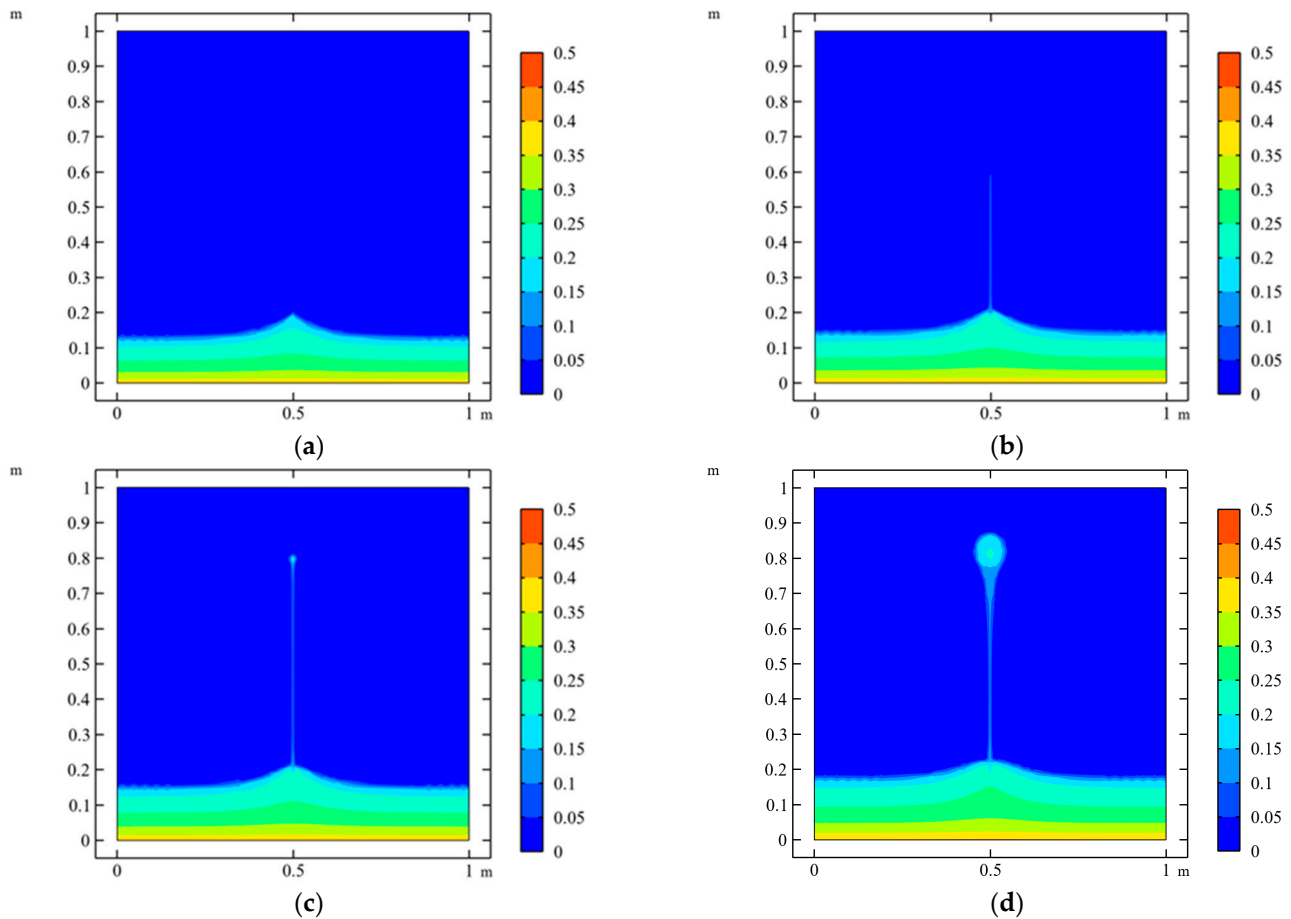


Figure 2. Verification model and the saturation distribution of the gas phase at different times: (a) 70, (b) 79, (c) 84, and (d) 100 s.

2.3. Numerical Simulation Scheme for the Influence of Single Fracture on Oil Vapor Leakage and Migration in Water-Sealed Oil Storage Caverns

2.3.1. Calculation Model

To investigate the influence of single fracture characteristic parameters on the migration characteristics of oil leaked oil vapor during the oil storage period of underground water-sealed oil storage caverns, a cavern model based on the model in Zhang et al. [22] was designed. The model, shown in Figure 3, consists of three main caverns and a series of water curtain holes. The model is 328 m long and 210 m high. The distance between the left cavern and the middle cavern is 30 m, and the distance between the middle cavern and the right cavern is 58 m. The lower boundary of the model is at elevation 0, the upper boundary is level with the average groundwater level at elevation 210 m, and an artificial water curtain is set at elevation 90 m. The water curtain holes are parallel to the axis of the cavern, have a diameter of 0.1 m, are spaced 10 m apart, and extend 16 m beyond the cavern wall on the left and right sides. The left and right boundaries of the model extend 90 m from the outside of the cavern wall, and the bottom boundary extends 60 m downward from the bottom of the cavern (to an elevation of 0 m). The mesh of the model is composed of quadrilateral and triangular elements, and the mesh between cracks, caverns, and water

curtain holes is properly densified. Prior to the simulation, a mesh dependence analysis was performed to ensure the accuracy of our results. The total number of elements in the final model is 19,403. The mesh, boundary conditions, and initial conditions used in the numerical calculation are shown in Figure 3.

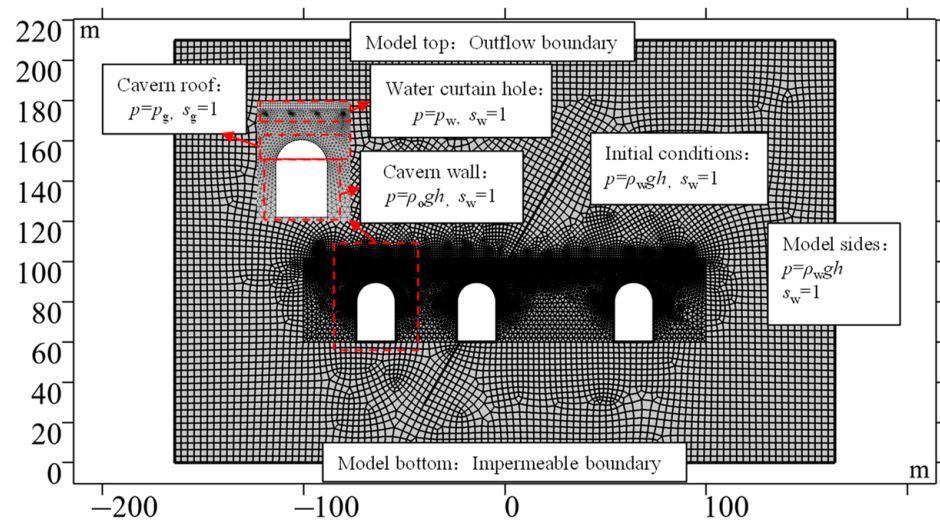


Figure 3. The mesh and boundary conditions of the calculation model.

2.3.2. Initial and Boundary Conditions

The initial conditions for the analysis were established as follows. Prior to the excavation of the cavern, the initial groundwater pressure in the seepage field was determined based on the hydrostatic pressure principles. After three years of excavation, the resulting seepage field and saturation distribution were used as the initial conditions for subsequent numerical simulations during the operation period. The oil vapor leakage and migration model was divided into two distinct physical fields, namely the Darcy seepage field and the phase transfer field in porous media, each requiring its own set of initial and boundary conditions.

Regarding the boundary condition for groundwater seepage, the left and right boundaries of the model were considered water head boundaries with the pressure of $P = \rho_w g(210 - y)$ m. Meanwhile, the top and bottom boundaries of the model were treated as zero flow boundaries. During the construction phase, the designed groundwater level of the cavern was set to 120 m from the top of the cavern, while the pressure of the water curtain hole was maintained at 150 kPa, and the boundary of the cavern was considered as having a pressure head of 0 m. When in oil storage conditions, the liquid oil product floats on the water cushion, and the saturated vapor occupies the upper part above the liquid oil. In this study, the thickness of the water cushion layer was neglected, and the density of the liquid oil was set as 850 kg/m^3 , while the saturated vapor pressure was set as 0.2 MPa. The boundaries of the vault, side wall, and floor of the cavern are determined based on the oil vapor pressure and the oil storage pressure, respectively.

In terms of the boundary conditions of the phase transfer field, the liquid phase boundaries were set at the left and right boundaries of the model, the water curtain hole, the side walls, and the floor of the cavern, while the gas phase boundary was established at the vault of the cavern. The bottom boundary of the model was treated as a no-flux boundary. Due to the possibility of oil vapor escaping into the atmosphere, the top boundary of the model was specified as an outflow boundary.

2.3.3. Parameter Values

The lithology of the reservoir area was classified as granitic gneiss. The cavern's rock mass exhibited a permeability coefficient (k) of $1.0 \times 10^{-9} \text{ m/s}$, and a porosity of

0.05. The densities of water (ρ_w) and gas (ρ_g) were 1000 and 3.125 kg/m³, respectively. The dynamic viscosities of water (μ_w) and gas (μ_g) were 1.0×10^{-3} and 2.0×10^{-5} Pa·s, respectively. Table 1 depicts the numerical calculation scheme used to explore the effects of various fracture parameters on the oil vapor migration, whereby five different values were evaluated for each parameter. For all scenarios, a storage duration of 50 years was analyzed, following three years of construction.

Table 1. Numerical calculation scheme for the parametric study.

Case	Fracture Permeability (k_f)/m ²	Fracture Width (d_f)/mm	Fracture Inclination (θ)/(°)	Distance from Fracture to Middle Cavern (s)/m
1	1.1×10^{-10} m ²			
2	1.1×10^{-11} m ²			
3	1.1×10^{-12} m ²	0.1	60	0
4	1.1×10^{-13} m ²			
5	1.1×10^{-14} m ²			
6		0.05		
7		0.075		
8	1.1×10^{-12} m ²	0.1	60	0
9		0.125		
10		0.15		
11			40	
12			50	
13	1.1×10^{-12} m ²	0.1	60	0
14			70	
15			80	
16				0
17				5
18	1.1×10^{-12} m ²	0.1	60	10
19				15
20				20

3. Results and Analysis

3.1. Effect of Fracture Permeability on the Migration of Leaked Oil Vapor

Figure 4 depicts the contour of oil vapor leakage distribution for Case 1 to Case 5 after 50 years of storage. It is observed that when the fracture permeability was 1.1×10^{-10} and 1.1×10^{-11} m², which is approximately 10^6 and 10^5 times higher than the surrounding rock permeability, the flow of groundwater in the fracture towards the cavern was substantial. In situations where the groundwater in the surrounding rock was insufficient to supply the fracture, the fracture became unsaturated. In Figure 4a,b, unsaturated fractures became the primary pathway for oil vapor leakage. When the fracture permeability was 1.1×10^{-12} m² (Case 3), which was still significantly higher than the surrounding rock permeability by a factor of 10^4 , the extent of oil vapor leaked along the fracture was not as pronounced as in Case 1 and Case 2. In contrast, when the fracture permeability decreased to 1.1×10^{-13} and 1.1×10^{-14} m², which was about 10^3 and 10^2 times the surrounding rock permeability, the flow of groundwater in the fracture to the cavern was minor, and the fracture was continuously replenished by the groundwater in the surrounding rock. As a result, the fracture remained fully saturated, and there was no leakage of oil vapor along the fracture.

Figure 5 shows the variation in oil vapor leakage range and leakage volume with fracture permeability after 50 years of oil storage. It can be seen from the figure that with the increase in fracture permeability, the oil vapor leakage range and leakage volume showed a trend of increasing slowly at first and then increasing rapidly. When the fracture permeability was less than 1.1×10^{-12} m², the oil vapor leakage range and leakage volume did not change significantly with the increase in fracture permeability. However, when the fracture permeability was greater than 1.1×10^{-12} m², the range and amount of oil vapor leakage changed significantly with the increase in fracture permeability. In particular,

when the fracture permeability increased from 1.1×10^{-11} to $1.1 \times 10^{-10} \text{ m}^2$, the range of oil vapor leakage increased from 3484.9 to 9248.1 m^2 , with an increase of 165.4%. The amount of oil vapor leakage increased from 22.70 to 128.09 m^2 , with an increase of 464.3%. This indicates that the increase in the permeability of the single fracture causes the increase in the range and amount of oil vapor leakage, causing the unsaturated high-permeability fracture to become the main channel for oil vapor leakage. Therefore, when there are fractures with high permeability in the underground cavern reservoir area, corresponding engineering measures should be taken to avoid oil vapor leakage along the unsaturated fractures, which will bring serious environmental and safety problems.

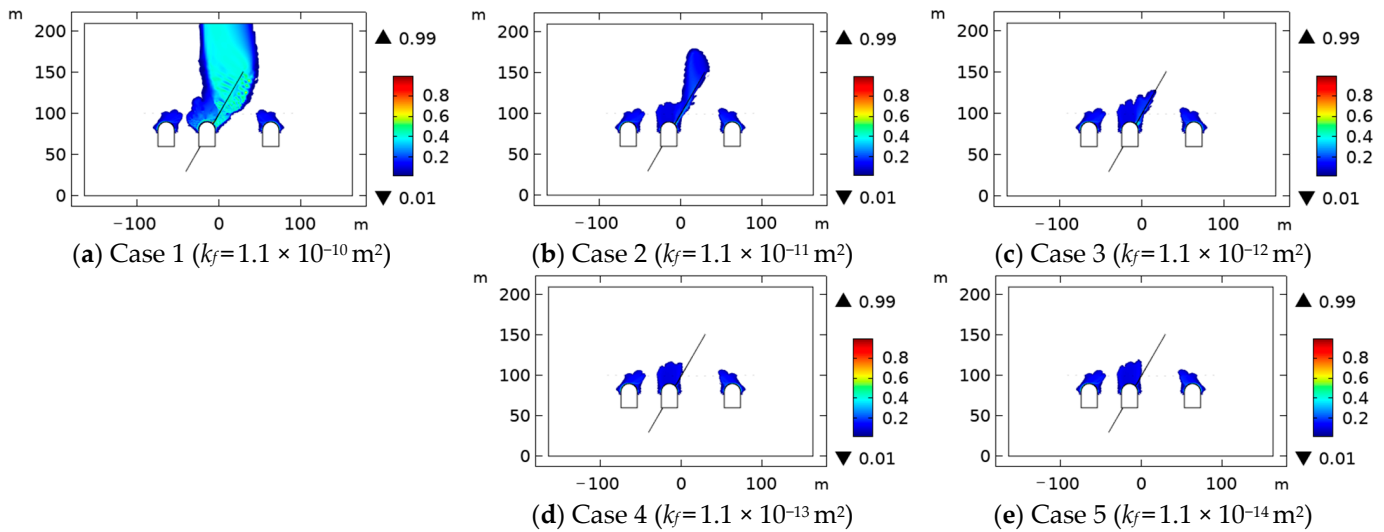


Figure 4. Contour of oil vapor leakage distribution for different cases after 50 years of oil storage.

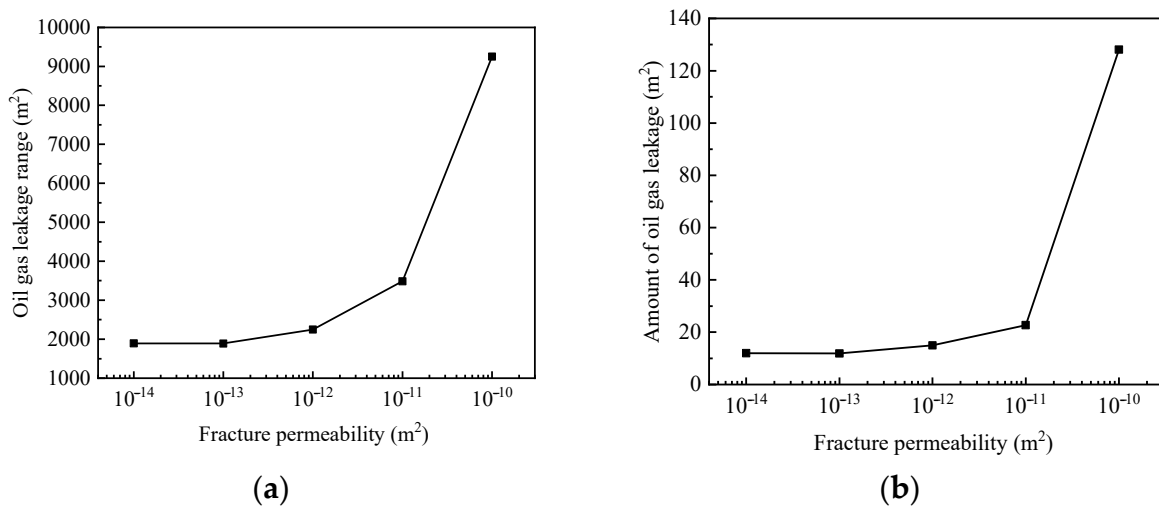


Figure 5. The variation in (a) oil leakage range and (b) amount of oil leakage versus fracture permeability.

3.2. Effect of Fracture Width on the Migration of Leaked Oil Vapor

Figure 6 is the contour of oil vapor leakage range distribution after 50 years of storage for Case 6 to Case 10. It is evident from the figure that leaked oil vapor migrating along fractures occurred in all cases after 50 years of the oil storage operation. This indicates that the spatial distribution of oil vapor migration is affected by the presence of fractures. With the increase in fracture width, the phenomenon of oil vapor leakage along fractures becomes more prominent, and the range of oil vapor leakage also expands. This is because wider fractures have a greater water-conducting ability. In the absence of a timely groundwater

supply near the fracture, the fracture becomes the primary channel for oil vapor leakage and migration. Thus, maintaining the fractures in a saturated state is crucial in preventing oil vapor leakage and migration along the fractures.

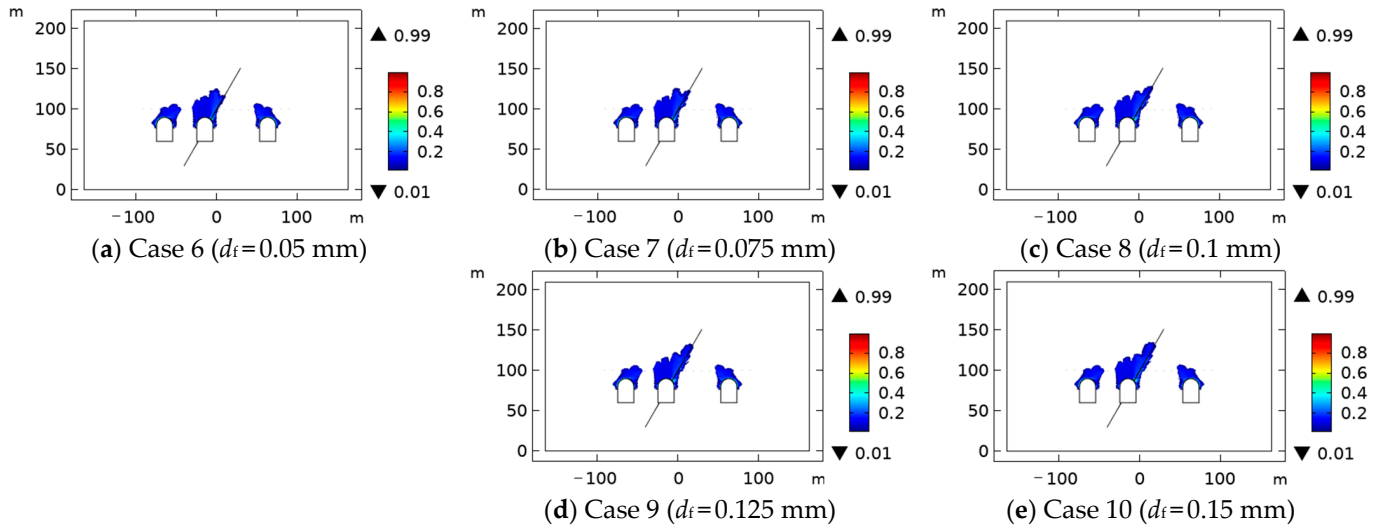


Figure 6. Contour of oil vapor leakage distribution for different cases after 50 years of oil storage.

Figure 7 displays a graph depicting the variation in parameters of oil vapor leakage with fracture width after the 50 years oil storage period. As the width of the fracture increased, both the range and amount of oil vapor leakage also increased, indicating a “linear” relationship. For instance, when the fracture width was 0.05 mm, the range of oil vapor leakage spanned 2115.3 m², with a volume of 13.944 m³. Conversely, when the fracture width increased to 0.15mm, the range of oil vapor leakage grew to 2358.8 m², with a volume of 15.721 m³.

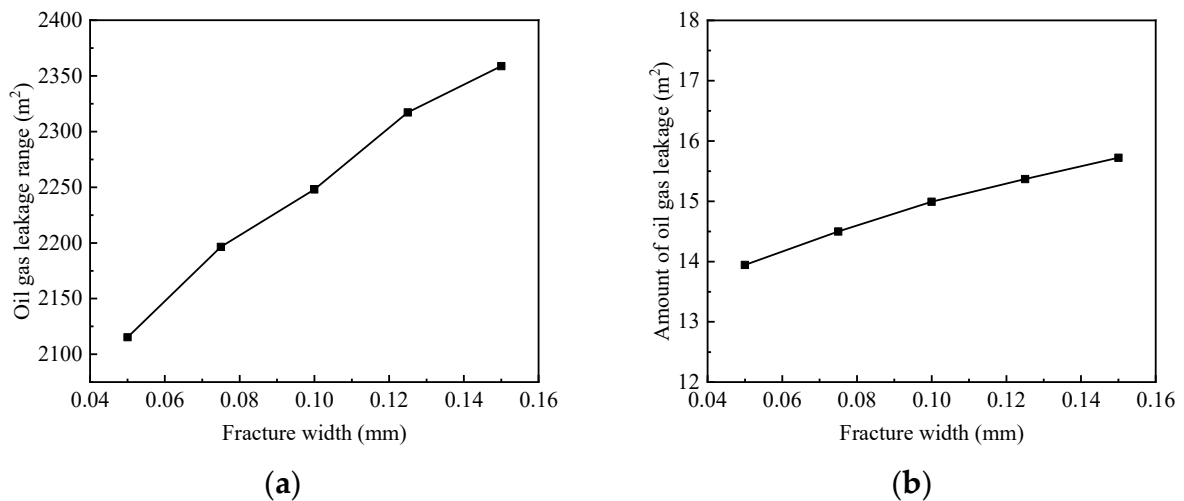


Figure 7. Variation in (a) range of oil vapor leakage; and (b) amount of oil vapor leakage versus fracture width.

3.3. Effects of Fracture Inclination on the Migration of Leaked Oil Vapor

Figure 8 is the contour of oil vapor leakage distribution after 50 years of storage for Case 11 to Case 15. As the fracture inclination increased, leaked oil vapor migrating along the fracture became more obvious. This is because the larger the inclination angle of the fracture, the faster the groundwater flowed along the fracture. When the groundwater in

the surrounding rock mass cannot be replenished in time, the fracture becomes unsaturated, and oil vapor spreads more easily.

Figure 9 shows the variation in oil vapor leakage parameters with fracture inclination angle after 50 years of oil storage. The overall trend of oil vapor leakage range and leakage volume during the oil storage period does not vary significantly, with a slight increase, as the fracture inclination angle increases. For example, at a fracture inclination angle of 40°, the oil vapor leakage range covers 2212.8 m², with a corresponding leakage volume of 14.342 m³. Comparatively, with a fracture inclination angle of 80°, the oil vapor leakage range increases to 2278.7 m², with a leakage volume of 15.054 m³. These observations are consistent with the findings presented in Figure 8. Moreover, The data further reveals that the fracture inclination has very little impact on the leakage volume of oil vapor. It only affects the distribution of oil vapor.

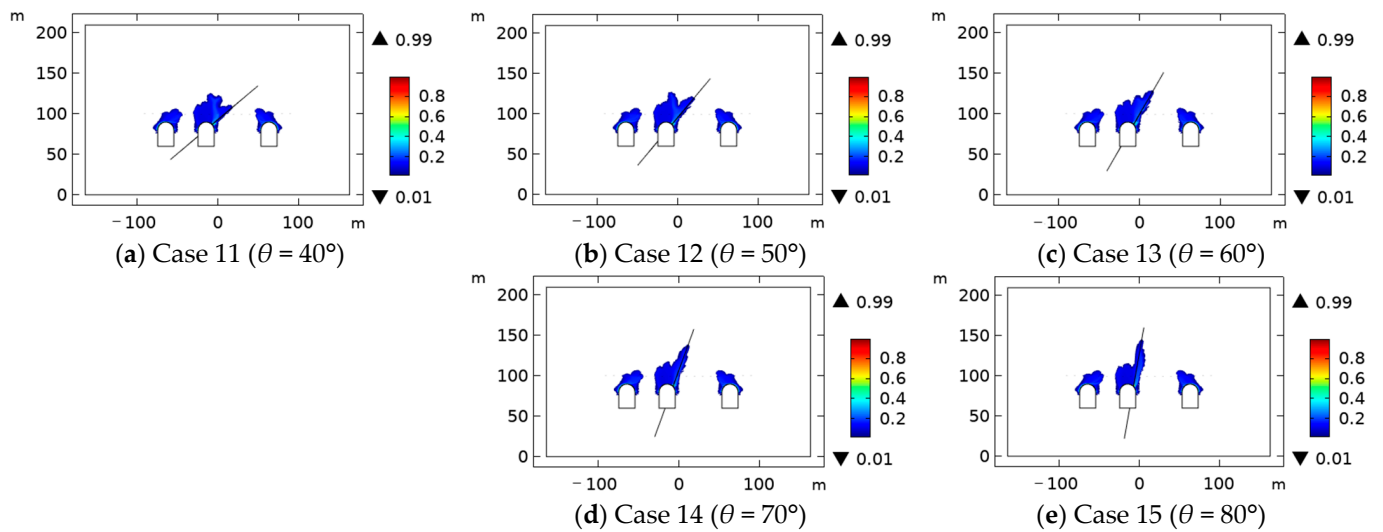


Figure 8. Contour of oil vapor leakage distribution for different cases after 50 years of oil storage.

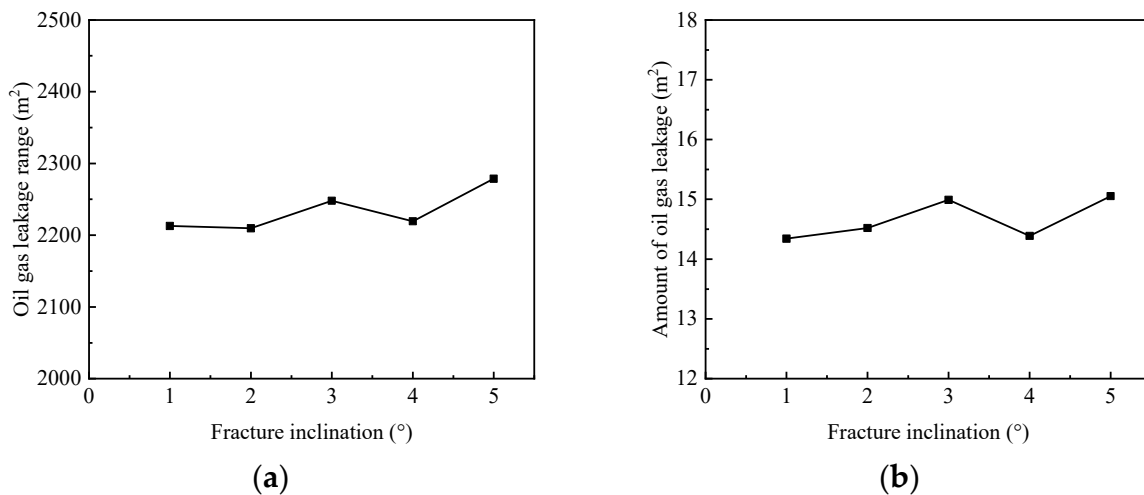


Figure 9. Variation in (a) range of oil vapor leakage; and (b) amount of oil vapor leakage versus fracture inclination.

3.4. Effects of Fracture Position on the Migration of Leaked Oil Vapor

Figure 10 shows the contour of the range distribution of leaked oil vapor after 50 years of storage for Cases 16 to 20. It can be observed that when the fracture passed through the cavern, the fracture was the main oil vapor diffusion channel, and the oil vapor was

distributed in a large area around the fracture (Figure 10a). As the distance between the fracture and the cavern increased, the leakage of oil vapor along the fracture became less obvious. When the fracture is located outside the cavern, oil vapor will not leak along the fracture (Figure 10d,e).

Figure 11 is the variation curve of the oil vapor leakage range and leakage volume with the distance from the fracture to the middle cavern when the cavern oil storage operation is 50 years. As the distance between the fracture and the cavern in the middle increased, the range and amount of oil vapor leakage decreased rapidly. It can be seen that only when the fracture ran through the cavern was oil vapor most likely to diffuse, but when the fracture was not connected to the cavern, oil vapor was not easy to diffuse. This also shows the importance of sealing cracks in the surrounding rock of the oil depot. When the distance between the fracture and the middle cavern exceeded 5 m, the slope of the curve of the oil vapor leakage range and leakage rate gradually became flat, and the change in the oil vapor leakage range and leakage rate was small.

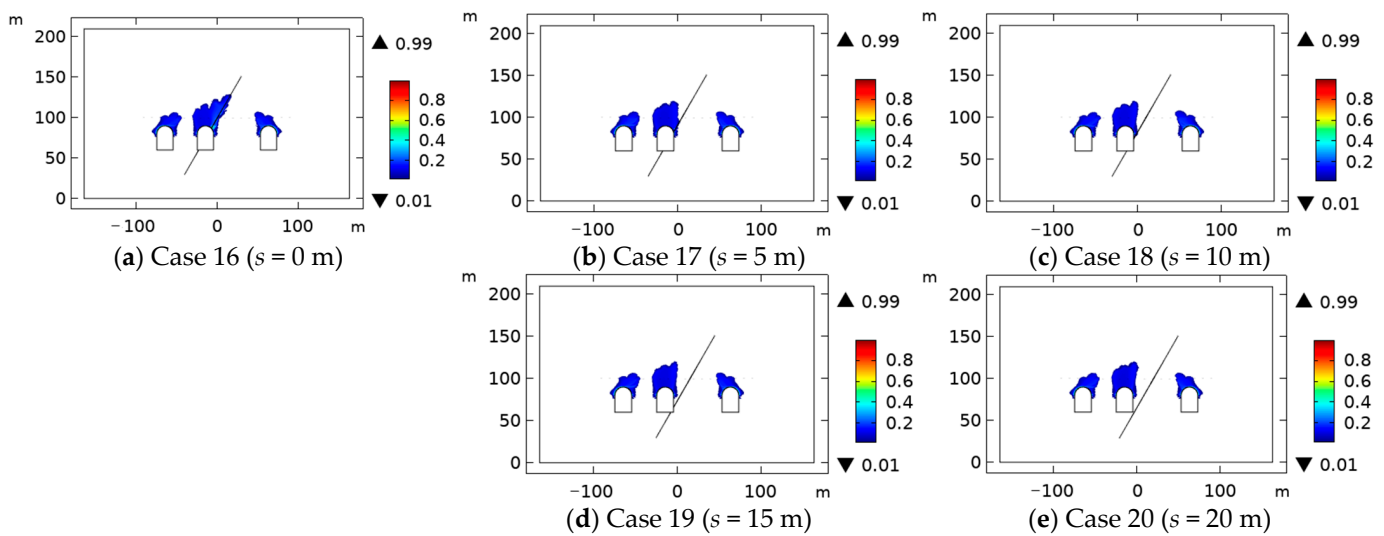


Figure 10. Contour of oil vapor leakage distribution for different cases after 50 years of oil storage.

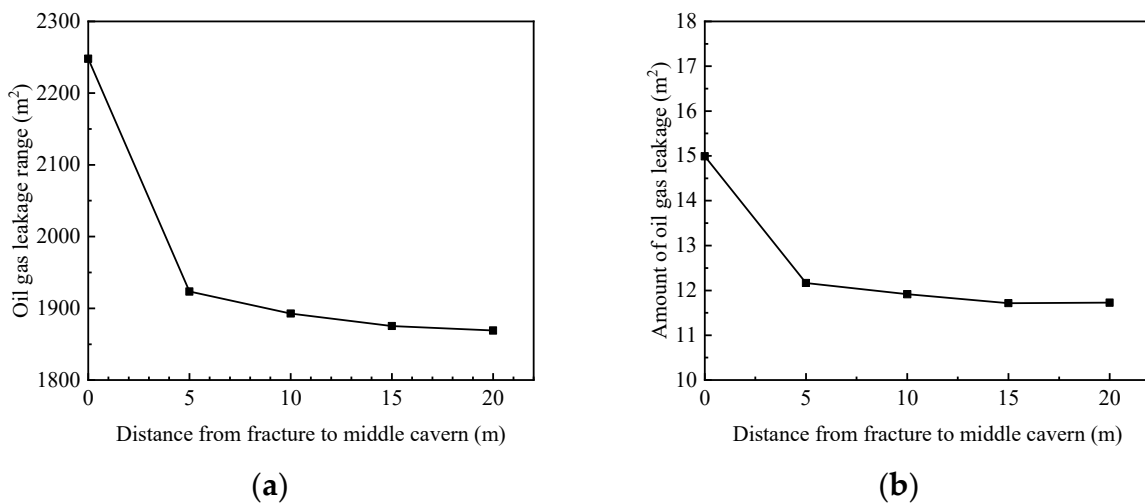


Figure 11. Variation in (a) range of oil vapor leakage; and (b) amount of oil vapor leakage versus distance from fracture to the middle cavern.

4. Engineering Application

4.1. Project Overview

The National Petroleum Reserve Huangdao underground water-sealed cavern project is a large-scale underground oil storage facility with a designed capacity of $300 \times 104 \text{ m}^3$. The project consists of nine main caverns, which are arranged in parallel at an angle of 45° from north to west. The underground project is mainly composed of the main caverns, shafts, water curtain systems, and construction roadways. The main caverns are divided into three groups, each with three caverns, for a total of nine caverns. Each group of caverns is connected by construction roadways. The caverns are circular arched holes with vertical sidewalls. They have a span of 20 m, a height of 30 m, a length between 484 and 717 m, and a floor elevation of -50.0 m . A water curtain system is installed 25 m above the top of the cavern group. It consists of water injection roadways and water curtain holes. The distance between the water curtain holes is 10 m, the diameter of the water curtain holes is 120 mm, and the pressure of the water curtain system is 300 kPa. The water curtain system covers the entire cavern area.

4.2. Fracture Network Model

The oil depot area is a granite landform with F3, F7, and F8 faults and fractured zones. According to the survey results of the Huangdao underground cavern site area, the distribution of faults and the origin of structural planes, and the principle of similarity in the area and differences in intervals, the structural plane of the oil depot area can be divided into five areas. To facilitate problem analysis, this paper selected a group of typical cross-sections of a group of caverns located in Zone IV of Huangdao underground water-sealed caverns to carry out a numerical simulation of oil vapor leakage and migration during the storage period. Regardless of construction roadways and shafts, the selected sections were calculated as shown in Figure 12.

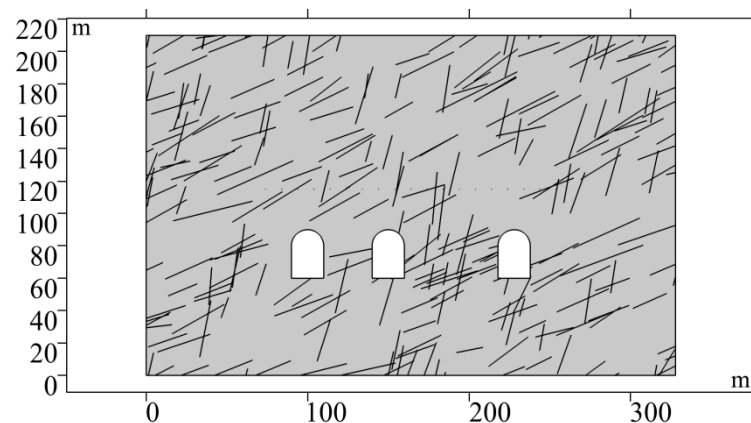


Figure 12. Fracture network model in Zone IV of Huangdao Oil Depot.

According to the data, Zone IV was mainly near the SN direction, with $NE45^\circ \sim NE60^\circ$ and $NE30^\circ$ structural planes. In addition, according to the statistical data of structural planes in the region, it was found that the overall trend of the cavern area was from $NW330^\circ \sim NW345^\circ$ to $NE45^\circ \sim NE60^\circ$. According to the geological survey of the reservoir site area and the statistical results of on-site joints and fissures, the inclination angles of joints and fissures in the analysis area were mostly $20^\circ \sim 40^\circ$, $55^\circ \sim 80^\circ$; the joint density was 0.35–1.50 pieces/m. The depth was about 1 bar/m. According to the above actual engineering geological survey results in the reservoir area, the geostatistical fracture parameters of Zone IV of Huangdao Oil Depot obtained in the model are shown in Table 2.

Table 2. Parameters of model fractures in Zone IV of Huangdao Oil Depot.

No. of Fracture Group	Density	Inclination		Trail Length	
		Mean (Degree)	Standard Deviation (Degree)	Mean (mm)	Standard Deviation (mm)
1	0.001	76	5	24	6.4
2	0.002	24	6	28	7.8

According to the fracture parameters in Table 2, a two-dimensional random fracture network model generation program that can directly call COMSOL was written in MATLAB. The program uses the Monte Carlo method to generate a random fracture network with the desired properties. The fracture network model of Zone IV of the Huangdao Oil Depot was established using this program (as shown in Figure 12). The numerical simulation of oil vapor leakage and migration was carried out on the fracture network model using COMSOL Multiphysics. The boundary conditions and initial conditions were the same as in Section 2.3.2.

4.3. Calculation Result Analysis

Figure 13 shows a cloud map of the distribution of oil vapor leakage after different storage periods in Zone IV of the Huangdao underground water-sealed cavern. The figure shows that after the oil storage operation in the cavern, a certain range of oil vapor pollution circles was formed on the surrounding rocks at the top of the caverns. With the increase in oil storage time, the area of the oil vapor pollution circles also increased.

The figure also shows that the range of oil vapor leakage above the middle cavern was larger than that of the left and right two caverns. This was because the top of the middle cavern intersects with the fissures. The high-permeability fissures became the main channel for oil vapor leakage and migration, which accelerated the migration of oil vapor leakage, which led to an increase in the area of the oil vapor leakage pollution circle.

Figure 14 shows a graph of the relationship between oil vapor leakage parameters and oil storage operation time during the oil storage period in Zone IV of the Huangdao underground water-sealed cavern. The figure shows that with the increase in oil storage time, the range of oil vapor leakage, leakage volume, and the longest vertical leakage distance all increase. All three parameters had a positive power function relationship with the oil storage operation time as a whole. The fitting formulas were:

- Range of oil vapor leakage: $A = 497.29t^{0.1}$
- Leakage volume: $Q = 5.37t^{0.03}$
- Longest vertical leakage distance: $Y = 7.56t^{0.12}$

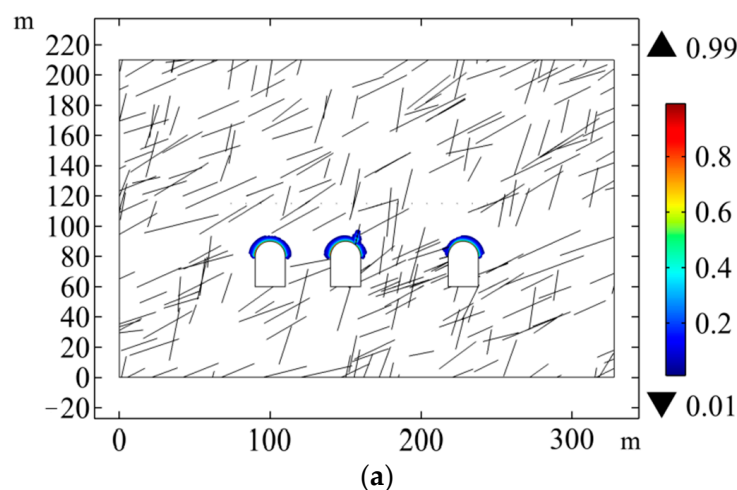


Figure 13. Cont.

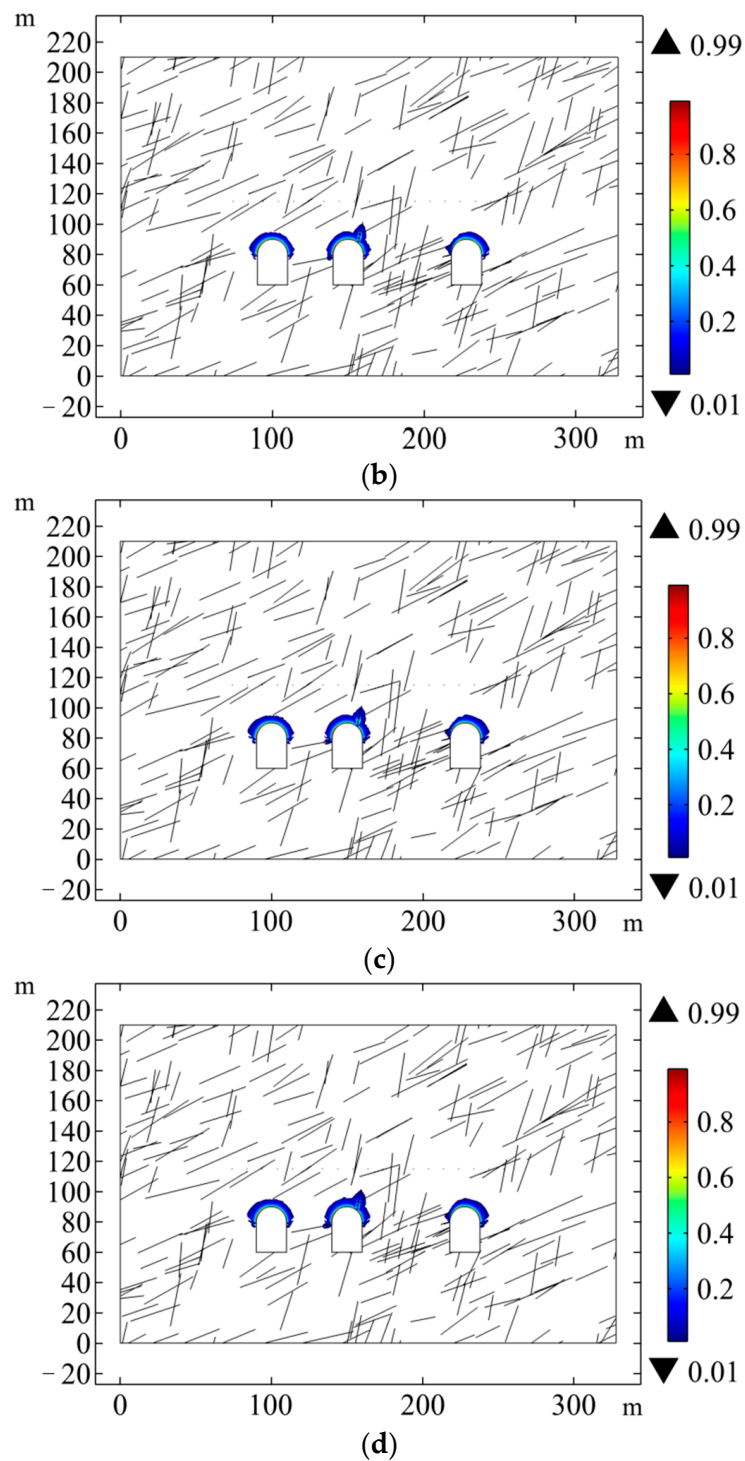


Figure 13. Cloud map of oil vapor leakage range distribution after an oil storage period of (a) 1a, (b) 10a, (c) 30a, and (d) 50 years.

The coefficient of determination (R^2) for all three equations was greater than 0.88, which indicates that the fitting formulas can accurately describe the variation trend of the oil vapor leakage range, leakage volume, and the longest vertical leakage distance during the oil storage period.

After 10 years, the trend of oil vapor leakage parameters gradually flattened out. This is because the oil storage caverns are lined with a water curtain system that prevents groundwater infiltration and oil leakage.

It is important to note that the fitting formulas presented here are only applicable to the Huangdao Oil Depot. Other projects may require different fitting formulas.

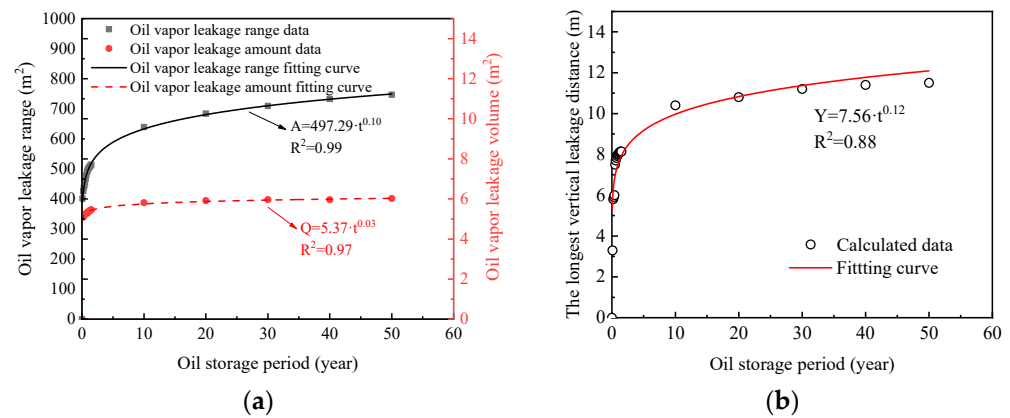


Figure 14. (a) Oil vapor leakage range, leakage volume, and (b) the longest vertical leakage distance during the oil storage period.

5. Discussions

To address the issue of oil vapor leakage migration, it is necessary to consider the following viewpoint: If the leakage of oil vapor in the groundwater sealing oil reservoir can be effectively controlled for a period of 50 years of oil storage operations while remaining within an acceptable range, then the environmental and safety concerns arising from oil vapor leakage would be limited. Based on our research findings, it appears that the parameters associated with oil vapor leakage exhibit a minimal change in the later stages of oil storage, indicating the possibility of identifying this acceptable value.

Determining a reasonable maximum allowable oil vapor leakage range or leakage value requires the consideration of two key aspects. Firstly, the safety of the water seal in the oil storage depot must be taken into account. Secondly, the economic factors related to the water seal in the oil storage depot need to be considered as well. Overemphasizing the safety of the water seal in the cavern reservoir can result in high operating costs for the water curtain system, imposing a significant burden. Additionally, maintaining high water injection pressure in the water curtain holes can lead to a substantial increase in groundwater inflow into the cavern reservoir, affecting its oil reserve capacity. Moreover, the subsequent costs associated with treating oil-contaminated water in the cavern reservoir would also increase significantly. Conversely, placing excessive emphasis on the water seal economy of the cavern reservoir would result in a low operating cost for the water curtain system, reducing the burden. However, this may lead to a situation where the groundwater pressure above the cavern roof becomes lower than the oil vapor pressure in the reservoir. As a result, the oil vapor within the reservoir may drive groundwater flow in the surrounding rock mass above the cavern roof, leading to oil vapor leakage into the surrounding rock mass and potentially into the atmosphere. Such leaks could pose health, safety, and environmental risks. Therefore, determining a reasonable maximum allowable oil vapor leakage range or leakage value is of great importance and significance for similar groundwater sealing oil depot projects. Future research endeavors can explore this topic from the perspective of water seal safety and economy in order to identify the maximum allowable oil vapor leakage range or leakage value.

Currently, the commonly employed methods for controlling gas leakage in underground caverns include chamber lining, freezing methods, surrounding rock grouting, and the use of natural groundwater and artificial water curtains. Techniques such as perimeter grouting, cavern lining, and freezing, which rely on permeability control methods to achieve leakage control, are time-consuming and economically unfavorable. Past engineering experiences have demonstrated that the most effective way to control gas leakage is through the use of artificial water curtains for hydrodynamic control. The reason artificial

water curtains can seal the gas within the cavern is that they induce groundwater to flow toward the cavern through cracks in the surrounding rock. If the hydraulic gradient of the seepage field exceeds a certain critical value, the gas in the cavern will not enter the cracks in the surrounding rock mass, or any gas bubbles that have entered the cracks will not move outward. This critical value represents the maximum allowable leakage range or leakage amount mentioned earlier. Determining this value is a topic that requires further study and exploration.

6. Conclusions

This paper examines the impact of fracture parameters on oil vapor leakage and migration characteristics during the storage period in underground water-sealed caverns. The study utilized the theory of two-phase flow in porous media and developed a fracture–pore dual-media two-phase flow model, which was validated using weak-form partial differential equations (PDEs). The model was subsequently employed to analyze the Huangdao Oil Depot, focusing on the influence of fracture parameters on oil vapor leakage and migration characteristics. The findings of the study led to the following conclusions:

(1) The fracture permeability (k_f), fracture width (d_f), fracture dip angle (θ), and oil vapor leakage parameters (oil vapor leakage range and leakage amount) were positively correlated, while the distance (s) between the fracture and the middle cavern was negatively correlated with oil vapor leakage parameters (oil vapor leakage range and leakage amount);

(2) Through sensitivity analysis, taking oil vapor leakage range and leakage volume as evaluation indicators, the relative influence of fracture geometry parameters on the oil vapor leakage and migration process during the oil storage period of the underground water-sealed oil depot was in the following order: $k_f > d_f > s > \theta$;

(3) Based on the statistical data of the actual geological fractures of the Huangdao underground oil depot, a two-dimensional fracture network model was generated. The results showed that the oil vapor leakage parameters had a positive power function relationship with the oil storage operation time, and the oil vapor leakage parameters had a large change trend in the early stage of oil storage in caverns, and gradually decreased in the later stages.

The findings of this study have important implications for the design and construction of underground oil storage caverns. The gas–liquid two-phase flow model of fracture–pore dual medium in fractured rock mass developed in this study could offer a numerical simulation tool to assess and mitigate the risk of oil vapor leakage.

Author Contributions: D.T.: conceptualization, writing—original draft preparation. H.J.: methodology, software, validation. M.S.: resources. Z.J.: writing—review and editing. All authors have read and agreed to the published version of the manuscript.

Funding: This research was jointly supported by the National Natural Science Foundation of China, grant number 52109112, the Natural Science Foundation of Hunan Province, grant number 2022JJ30606, the Scientific Research Project of Hunan Provincial Department of Education, grant number 21B0321, the Hunan Province Natural Resources Research Project, grant number 2022-31, and the Open Fund of Zhejiang Key Laboratory of Marine Geotechnical Engineering and Materials, grant number OGME21006.

Institutional Review Board Statement: Not applicable.

Informed Consent Statement: Not applicable.

Data Availability Statement: Data are contained within the article.

Conflicts of Interest: The authors declare no conflict of interest.

References

1. Lu, M. Finite element analysis of a pilot gas storage in rock cavern under high pressure. *Eng. Geol.* **1998**, *49*, 353–361. [[CrossRef](#)]
2. Mawire, A. Experimental and simulated thermal stratification evaluation of an oil storage tank subjected to heat losses during charging. *Appl. Energ.* **2013**, *108*, 459–465. [[CrossRef](#)]

3. Ravandi, E.G.; Rahmannedjad, R.; Karimi-Nasab, S.; Sarrafi, A. Application of Numerical Modelling and Genetic Programming in Hydrocarbon Seepage Prediction and Control for Crude Oil Storage Unlined Rock Caverns. *Geofluids* **2017**, *2017*, 6803294. [[CrossRef](#)]
4. Qiao, L.; Li, S.; Wang, Z.; Tian, H.; Bi, L. Geotechnical monitoring on the stability of a pilot underground crude-oil storage facility during the construction phase in China. *Measurement* **2016**, *82*, 421–431. [[CrossRef](#)]
5. Gao, B.; Pan, D.D.; Xu, Z.H.; Zhang, L.W.; Zhao, S.L. Effect of density, trace length, aperture, and direction angle on permeability performance of fracture networks. *Int. J. Geomech.* **2020**, *20*, 04020116. [[CrossRef](#)]
6. Liu, W.; Zhang, Z.; Fan, J.; Jiang, D.; Li, Z.; Chen, J. Research on gas leakage and collapse in the cavern roof of underground natural gas storage in thinly bedded salt rocks. *J. Energy Storage* **2020**, *31*, 101669. [[CrossRef](#)]
7. Chen, X.; Li, Y.; Jiang, Y.; Liu, Y.-X.; Zhang, T. Theoretical research on gas seepage in the formations surrounding bedded gas storage salt cavern. *Petrol. Sci.* **2022**, *19*, 1766–1778. [[CrossRef](#)]
8. Hu, C.; Chen, G.; Yang, R.; Tang, L.; Luo, Y. A case study on optimum identification of water curtain hydraulic pressure using three-phase flow numerical simulation. *Environ. Earth Sci.* **2019**, *78*, 300. [[CrossRef](#)]
9. Gao, X.F.; Zhang, Y.J.; Hu, Z.J.; Huang, Y. Numerical investigation on the influence of surface flow direction on the heat transfer characteristics in a granite single fracture. *Appl. Sci.* **2021**, *11*, 751. [[CrossRef](#)]
10. Yamamoto, H.; Pruess, K. Numerical Simulations of Leakage from Underground LPG Storage Caverns. Ph.D. Thesis, University of California, Berkeley, CA, USA, 2004.
11. Shi, H.B. Analysis and Evaluation of Water Sealing Conditions and Surrounding Rock Stability of Underground Water-Sealed Caverns in Huangdao. Ph.D. Thesis, Beijing Jiaotong University, Beijing, China, 2010.
12. Wang, T.; Yang, C.; Ma, H.; Daemen, J.; Wu, H. Safety evaluation of gas storage caverns located close to a tectonic fault. *J. Nat. Gas. Sci. Eng.* **2015**, *23*, 281–293. [[CrossRef](#)]
13. Tan, L. Study on the Influence of Fractured Rock Mass Structure of a Groundwater-Sealed Cavern in Yantai on the Stability of Surrounding Rock and Water Sealing Conditions. Ph.D. Thesis, China University of Geosciences, Wuhan, China, 2021.
14. Ren, F.; Ma, G.; Wang, Y.; Fan, L. Pipe network model for unconfined seepage analysis in fractured rock masses. *Int. J. Rock. Mech. Min.* **2016**, *88*, 183–196. [[CrossRef](#)]
15. Ren, F.; Ma, G.; Wang, Y.; Fan, L.; Zhu, H. Two-phase flow pipe network method for simulation of CO₂ sequestration in fractured saline aquifers. *Int. J. Rock. Mech. Min.* **2017**, *98*, 39–53. [[CrossRef](#)]
16. Lin, F.; Ren, F.; Luan, H.; Ma, G.; Chen, S. Effectiveness analysis of water-sealing for underground LPG storage. *Tunn. Undergr. Space Technol.* **2016**, *51*, 270–290. [[CrossRef](#)]
17. Javadi, M.; Sayadi, S. Stochastic discontinuum analysis of hydrocarbon migration probability around an unlined rock cavern based on the discrete fracture networks. *Tunn. Undergr. Space Technol.* **2018**, *81*, 41–54. [[CrossRef](#)]
18. Wijeratne, D.E.N.; Halvorsen, B.M. Computational study of fingering phenomenon in heavy oil reservoir with water drive. *Fuel* **2015**, *158*, 306–314. [[CrossRef](#)]
19. Vasheghani Farahani, M.; Foroughi, S.; Norouzi, S.; Jamshidi, S. Mechanistic study of fines migration in porous media using lattice Boltzmann method coupled with rigid body physics engine. *J. Energy Resour. Technol.* **2019**, *141*, 123001. [[CrossRef](#)]
20. Movahedi, H.; Vasheghani Farahani, M.; Masihi, M. Development of a Numerical Model for Single-and Two-Phase Flow Simulation in Perforated Porous Media. *J. Energy Resour. Technol.* **2020**, *142*, 042901. [[CrossRef](#)]
21. Brooks, R.H.; Corey, A.T. Hydraulic properties of porous media. In *Hydrology Papers*; Colorado State University: Fort Collins, CO, USA, 1964; pp. 1–27.
22. Zhang, B.; Li, W.; Feng, F.; Wu, B.; Cao, X. Numerical simulation for fluid-solid coupling characteristics in surrounding rock of underground water-sealed oil storage based. *J. Eng. Geol.* **2012**, *20*, 789–795.

Disclaimer/Publisher’s Note: The statements, opinions and data contained in all publications are solely those of the individual author(s) and contributor(s) and not of MDPI and/or the editor(s). MDPI and/or the editor(s) disclaim responsibility for any injury to people or property resulting from any ideas, methods, instructions or products referred to in the content.